DISCOVERING NONLINEAR PDES FROM SCARCE DATA WITH PHYSICS-ENCODED LEARNING

Anonymous authors
Paper under double-blind review

ABSTRACT

There have been growing interests in leveraging experimental measurements to discover the underlying partial differential equations (PDEs) that govern complex physical phenomena. Although past research attempts have achieved great success in data-driven PDE discovery, the robustness of the existing methods cannot be guaranteed when dealing with low-quality measurement data. To overcome this challenge, we propose a novel physics-encoded discrete learning framework for discovering spatiotemporal PDEs from scarce and noisy data. The general idea is to (1) firstly introduce a novel deep convolutional-recurrent networks, which can encode prior physics knowledge (e.g., known terms, assumed PDE structure, initial/boundary conditions, etc.) while remaining flexible on representation capability, to accurately reconstruct high-fidelity data, and (2) then perform sparse regression with the reconstructed data to identify the analytical form of the governing PDEs. We validate our proposed framework on three high-dimensional PDE systems. The effectiveness and superiority of the proposed method over baselines are demonstrated.

1 INTRODUCTION

Deriving analytical laws of physical phenomena is significant for understanding the dynamical patterns and complex spatiotemporal behaviors in nature. In the meanwhile, these formulated governing equations contribute to the establishment of scientific disciplines and the rapid development of technology. In general, scientists seek to find the underlying governing equations by rigorously following the first principles, including the conservation laws, geometric brownian motion assumptions and knowledge-based deductions. However, these classical approaches show limited capability and slow progress in identifying clear analytical governing equations, and leave numerous complex systems under-explored. Thanks to the recent achievements in machine learning (ML), the research work in the field of scientific discovery can be drastically accelerated.

The pioneer works (Bongard & Lipson, 2007; Schmidt & Lipson, 2009) apply the symbolic regression to reveal the underlying differential equations that govern the nonlinear physical systems without any prior background knowledge. Although this inspiring investigation implies the dawn of discovering the fundamental principles automatically in scientific ML, the scalability and overfitting issues herein have been the critical concerns. Recently, a ground-breaking work of sparse identification of nonlinear Dynamics (SINDy) (Brunton et al., 2016) introduces the sparse regression into the discovery of parsimonious governing equations based on the assumption that the dynamical systems are essentially controlled by only few dominant terms, which evolves to promote the sparsity in the candidate functions. Furthermore, the introduction of spatial derivative terms and improved the sparsity-promoting algorithm of sequential threshold ridge regression (STRidge) makes SINDy is applicable to general PDE discovery (i.e., the PDE-FIND algorithm) (Rudy et al., 2017). However, due to the demanding requirement of derivative fitting via numerical differentiation, these sparse regression methods largely rely on high-quality measurement data, which is barely accessible in the real-world sensing. Therefore, there is an urgent need to address the issue of identifying the underlying governing equations from low-resolution (LR) and noisy measurement data. Very recently, many works attempt to relieve the pain by reconstructing the high-resolution (HR) scientific data from LR measurements and then discovering the governing laws, including robust low-rank discovery (Li et al., 2020a), physics-informed spline learning (Sun et al., 2021) and physics-informed deep learning (Chen et al., 2020). Nevertheless, the dominant reconstruction part lacks explicit physical

interpretability (i.e., grey-box model), which may induce the difficulty in optimization especially for high-dimensional PDE systems with delicate patterns.

Contributions. To overcome the challenges resulted from the noisy and LR measurements, we propose a novel physics-encoded deep learning framework (i.e., white-box model) for discovering the governing equations of physical systems. The main contributions of this paper are three-fold:

- We design a novel recurrent network architecture that is able to fit the spatiotemporal measurement data with high accuracy and physical consistency. Notably, this network is characterized with the capability to encode given physics knowledge (e.g., known terms, assumed PDE structure, initial/boundary conditions, etc.) so that the given physics as model prior is respected rigorously.
- Based on the proposed reconstruction network, we develop a hybrid optimization approach to discover spatiotemporal PDEs from noisy and LR measurements. Specifically, to determine the explicit form of underlying governing equations, sparse regression is performed by using HR prediction inferred from the model. Finally, through inheriting the PDE terms and coefficients from the sparse discovery, we conduct the fine-tuning step with the completely physics-based network to further improve the accuracy of the scientific discovery.
- The proposed coupled framework establishes the physics-encoded data-driven predictive model from the noisy and LR measurement. To evaluate the performance of the model, we perform three numerical experiments on a variety of nonlinear systems. It is found that the proposed approach demonstrates excellent robustness and accuracy in spite of the high level of noise and the scarcity (spatially and temporally) in the measurements.

2 Related work

Dynamical system modeling. Simulating multi-dimensional PDE systems with neural networks (NNs) has been a renewed research topic, which can be dated back to last century (Lee & Kang, 1990; Lagaris et al., 1998). Like the traditional simulation methods, the recent breakthrough in NN-based modeling for physical systems also fall into two streams: continuous and discrete learning. The continuous learning scheme can avoid the notorious demand of time-step and grid sizes for numerical stability. Among the meshfree strategies, based on the incorporation of prior knowledge of PDE systems, there exist two directions seeking for the approximation of simulation with DNNs, i.e., the pure data-driven approaches (Han et al., 2018; Long et al., 2018; Wang et al., 2020) and physics-informed learning (Yu et al., 2017; Raissi et al., 2019; Rao et al., 2021b; Karniadakis et al., 2021). The former option relies on large amounts of high-quality data, while the physics-informed ML only requires scarce or even no labeled data due to the enhancement from physical constraints. Besides, it is worthwhile to mention that the recent studies on neural operators (Li et al., 2020b; Lu et al., 2021; Patel et al., 2021) have exhibited the great potential of learning the nonlinear, meshfree and infinite-dimensional mapping with DNNs for physical systems.

Regarding the discrete learning scheme, the mesh-based methods play a dominant role in simulating complex high-dimensional PDE systems. Herein, the convolutional architectures are mainly applied for handling regular grids in steady-state problems (Zhu & Zabaras, 2018; Zhu et al., 2019) and spatiotemporal systems (Bar-Sinai et al., 2019; Geneva & Zabaras, 2020; Kochkov et al., 2021; Ren et al., 2021), as well as irregular domains by considering elliptic coordinate mapping (Gao et al., 2021a). Moreover, with the theoretical development of graph neural networks (GNNs) (Kipf & Welling, 2016; Bronstein et al., 2017; Battaglia et al., 2018), researchers seek for a new direction for geometry-adaptative learning of nonlinear PDEs with arbitrary domains (Belbute-Peres et al., 2020; Sanchez-Gonzalez et al., 2020a; Gao et al., 2021c). In addition to the common mesh-based approaches, the particle-based frameworks have been attracting a lot of interest in scientific modeling for physical systems, especially by employing GNNs (Li et al., 2018; Ummenhofer et al., 2019; Sanchez-Gonzalez et al., 2020b).

Scientific data augmentation. Scientific data are typically sparse, noisy and incomplete. Therefore, data augmentation has been an active research area and received massive attention in the scientific ML community, e.g., data reconstruction from sparse measurements (Raissi, 2018; Callaham et al., 2019; Erichson et al., 2020; Rao et al., 2021a), super-resolution (SR) (Stengel et al., 2020;

Gao et al., 2021b) and denoising (Fathi et al., 2018). Generally, based on the type of incorporated data, we categorize the existing data augmentation methods into two groups. The first one is to extract the coherent structure and correlation features as the basis by utilizing the sufficient high-quality datasets. For instance, in the context of SR, the majority of NN-based frameworks (Liu et al., 2020; Esmaeilzadeh et al., 2020; Fukami et al., 2021) aim to reconstruct the high-resolution (HR) full-field data from low-resolution (LR) measurements by employing HR ground truth reference as the constraint. Nevertheless, the second type of data augmentation takes advantage of the physics-based model and can accurately capture the high-fidelity dynamical patterns from the LR and noisy measurement data. The recent advances of physics-based learning models have shown the the great success of data augmentation for PDE systems with only sparse and noisy data (Raissi, 2018; Rao et al., 2021a) and even without any labeled data (i.e., only with PDEs) (Gao et al., 2021b).

Data-driven discovery. The data-driven discovery is also a renascent research attempt. The earliest work (Dzeroski & Todorovski, 1995) introduced the inductive logic programming to find the natural laws from experimental data. With the rapid advance of machine intelligence, the past three decades have seen a considerable amount of literatures growing up around the interplay between ML and scientific discovery. Essentially, two genres have been observed in distilling governing equations, with respect to the searching of candidate functions. Firstly, the natural and optimal solution to automatically identify the governing equations for dynamical systems is to learn a symbolic model from experimental data. Hence, symbolic regression (Schmidt & Lipson, 2009) and symbolic neural networks (SNN) (Sahoo et al., 2018; Kim et al., 2020) have been explored for inferring the physical models without any prior knowledge. In addition, GNN (Cranmer et al., 2020) has also been studied to identify the nontrivial relation due to its excellent inductive capability.

The second group manually defines a large library functions based on the prior knowledge, and utilizes the sparse-prompting algorithms to discover the parsimonious physics model efficiently. The most representative works are SINDy (Brunton et al., 2016) and PDE-FIND (Rudy et al., 2017) for ordinary differential equations (ODEs) and PDEs, respectively. Nevertheless, the standard sparse representation-based methods are limited to the high-fidelity experimental data, which is usually difficult and expensive to obtain. Hence, many recent efforts have been devoted to discover governing equations from scarce and noisy data (Li et al., 2020a; Sun et al., 2021; Chen et al., 2020).

3 METHODOLOGY

3.1 PROBLEM DESCRIPTION

To discover the explicit form of the governing equation for a given system from the measurement data is of significance for scientists to understand some underexplored processes. To formalize this problem, which is also known as the data-driven equation discovery, let us assume the multi-dimensional spatiotemporal system is described by

$$\mathbf{u}_t = \mathcal{F}\left(\mathbf{x}, t, \mathbf{u}, \mathbf{u}^2, \mathbf{u}_x, \mathbf{u}_y, \nabla^2\mathbf{u}, \cdots\right) \tag{1}$$

where $\mathbf{u} \in \mathbb{R}^{1\times n}$ denotes the state variable consisting of n components, and $\mathcal{F}$ parameterizes the dynamics of a system with the state variables and their derivatives. The objective of the data-driven equation discovery is to uncover the closed form of $\mathcal{F}$ provided time series measurements on some fixed spatial locations. Although this problem has been studied extensively for decades, the combinatorically large search space of the possible equation appears as one of the major obstacles that hinders the discovery of the governing equation from measurements. The existence of noise, as well as the coarse-sampling of the measurement, also adds to the difficulty of this problem. To address these challenges, we proposed a novel physics-encoded recurrent network that is able to reconstruct the high-fidelity solution from the noisy and LR measurements with the help of prior physics knowledge. We successfully combine this network with the sparse regression for discovering the explicit form of the governing PDE of dynamical systems.

3.2 PHYSICS-ENCODED NETWORK FOR DATA RECONSTRUCTION

To obtain the numerical derivatives for constructing the library matrix is crucial to the equation discovery with sparse regression. Due to the LR and the noise in measurements, to directly apply

the traditional finite difference (FD) onto the raw measurements may lead to inaccurate derivatives, which would significantly complicates the equation discovery. To handle this, we introduce a recurrent network architecture, namely the Physics-encoded Recurrent Convolutional Neural Network (PeRCNN) shown as Fig. 1(1a) and (1b), to establish the data-driven predictive model from measurements. PeRCNN consists of a fully convolutional (Conv) network as initial state generator (ISG) and a well designed Conv block, namely Π-block (product) for updating the state variables on high-resolution grid recurrently. Note that our network does not require any HR data as the "label" for training, which is fundamentally different from the classic super resolution (SR) task.

The overall network architecture mimics the forward Euler time stepping $\mathbf{u}_{k+1} = \mathbf{u}_k + \mathcal{F}(\mathbf{u}_k; \boldsymbol{\theta})\delta t$ where $\boldsymbol{\theta}$ parameterizes a series of operations for computing $\mathcal{F}$. Since we seek the predictive model for HR solution, the ISG component is introduced to generate a HR initial state from the noisy and LR measurement $\tilde{\mathbf{u}}_0$ for the recurrent computation. The recurrent Π-block is a major innovation of this network architecture to capture the dynamics of $\mathcal{F}$. As shown in Fig. 1(1b), the input state variable to Π-block would firstly be mapped to the hidden space through multiple parallel Conv layers, whose output would then be fused via the element-wise product operation. A Conv layer with kernel size of 1 (Lin et al., 2013) is subsequently used to linearly combine multiple channels into the output of desired number of channels. Mathematically, the operations in Π-block can be described by the function as follows

$$\hat{\mathcal{F}}(\mathbf{u}_k) = \sum_{c=1}^{N_c} f_c \cdot \left(\prod_{l=1}^{N_l} \mathcal{K}^{(c,l)} \circledast \mathbf{u}_k \right) \tag{2}$$

where N_c and N_l denote the numbers of channels and parallel Conv layers respectively; $\circledast$ denotes the Conv operation; (c, l) indicates the Conv filter $\mathcal{K}$ of l-th layer and c-th channel; f_c is the weight in 1×1 Conv layer while the bias is omitted for simplicity. Though the proposed Π-block is free of nonlinear activation layers seen in traditional deep network, we demonstrate in Appendix Section A that Π-block is an universal polynomial approximator to the nonlinear function $\mathcal{F}$. In addition, this network architecture features the capability to encode physics knowledge, such as the existing term in the PDE and I/BCs. As shown in Fig. 1(1b), a highway physics-based Conv layer[1] can be created to account for existing terms known *a priori* in the PDEs. In Appendix Section C, we demonstrate that such a highway connection can accelerate the training speed and improve the accuracy of the fitted model. In addition, the knowledge of I/BCs of the system can be encoded into the network through the customized padding in Conv operation.

3.3 Sparse discovery

Based on the reconstructed HR solution, we further employ the sparse discovery algorithm (Rudy et al., 2017) to distill the underlying governing equations. The sparse regression method roots on a critical observation that the right hand side (RHS) of Eq. (1) for the majority of natural systems consists of only a few terms, i.e., the $\mathcal{F}$ demonstrates sparsity in the space of possible functions. Given a library of candidate functions of $\mathcal{F}$, we can formulate the discovery of the governing equation as a regression problem. Let us define that the state variable $\mathbf{u} \in \mathbb{R}^{n_s \times n_t}$ is on n_s spatial locations and within n_t time steps. After flattening the state variable into a column vector $\mathbf{U} \in \mathbb{R}^{n_s \cdot n_t \times 1}$, a library $\boldsymbol{\Theta}(\mathbf{U}) \in \mathbb{R}^{n_s \cdot n_t \times s}$ that encompasses a pool of s candidate functions (e.g., linear, nonlinear terms, derivatives, etc.) can be constructed to represent the governing equations of physical systems. Each column in $\boldsymbol{\Theta}(\mathbf{U})$ represents a candidate function in $\mathcal{F}$, such as $\boldsymbol{\Theta}(\mathbf{U}) = [\mathbf{1}, \mathbf{U}, \mathbf{U}^2, \ldots, \mathbf{U}_x, \mathbf{U}_y, \ldots]$. Assuming that $\boldsymbol{\Theta}(\mathbf{U})$ has a sufficiently rich column space, the governing equation described by Eq. (1) can be rewritten as a linear system

$$\mathbf{U}_t = \boldsymbol{\Theta}(\mathbf{U})\boldsymbol{\Xi} \tag{3}$$

by using a sparse coefficient vector $\boldsymbol{\Xi} \in \mathbb{R}^{s \times 1}$. To compute a reasonable $\boldsymbol{\Xi}$ such that the sparsity of the vector is promoted while the regression error is small, the Sequential Threshold Ridge regression (STRidge) algorithm (Rudy et al., 2017) is considered in this paper. For a given tolerance that filters the entries of $\boldsymbol{\Xi}$ with small value, we can obtain a sparse representation of $\mathcal{F}$. STRidge algorithm iteratively searches for the optimal tolerance based on the selection criteria

$$\boldsymbol{\Xi}^* = \arg\min_{\boldsymbol{\Xi}} \{||\mathbf{U}_t - \boldsymbol{\Theta}(\mathbf{U})\boldsymbol{\Xi}||_2 + \gamma||\boldsymbol{\Xi}||_0\} \tag{4}$$

[1]This Conv layer with the corresponding finite difference filter would be freezed throughout the training.

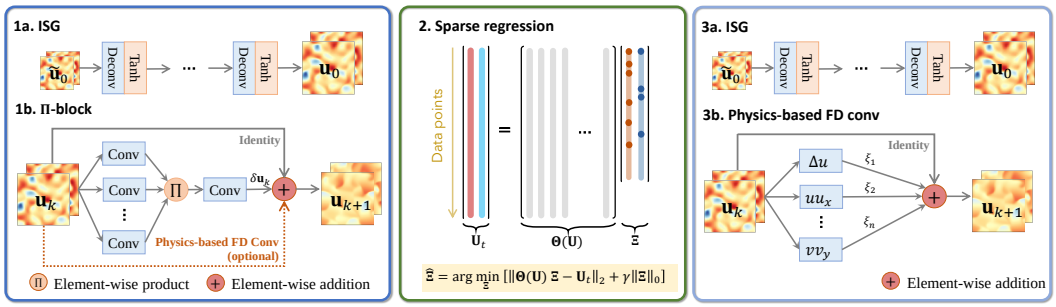

Figure 1: Discovery of governing PDEs with the proposed Physics-encoded DL framework. **1. Data reconstruction:** data-driven model constructed from noisy and LR measurement is used to generate HR solution for sparse regression; **2. Sparse regression:** STRidge algorithm is used to obtain the sparse coefficient vector $\boldsymbol{\Xi}$; **3. Coefficients fine tuning:** the PeRCNN built based on identified PDE structure is employed to fine-tune the coefficient from the sparse regression.

where $||\boldsymbol{\Xi}||_0$ is used to measure the sparsity of coefficient vector; $||\mathbf{U}_t - \boldsymbol{\Theta}(\mathbf{U})\boldsymbol{\Xi}||_2$ denotes the regression error; γ is the coefficient that balances the sparsity and the regression errors. Since the optimization objective has two components, we apply Pareto analysis to select an appropriate γ. The above procedure to find a sparse $\boldsymbol{\Xi}$ is also known as sparse regression.

3.4 Hybrid PeDL framework for equation discovery

In this part, we present the hybrid and coupled scheme of the proposed PeRCNN and the sparse regression for discovering the governing PDEs. As shown in Fig. 1, the whole equation discovery process can be divided into three stages, including the data reconstruction, the sparse regression and the fine-tuning of coefficients. The proposed framework enables us to iterate over these three stages to keep refining the result until convergence. The purpose of each stage, as well as the technical details, would be detailed as follows.

Data reconstruction. Since the experimental measurements are typically sparse and noisy, we firstly utilize the PeRCNN introduced in Section 3.2 to reconstruct the high-fidelity data in order to obtain accurate derivative terms in the stage of sparse regression. Given the measurement $\tilde{\mathbf{u}} \in \mathbb{R}^{n_t' \times H' \times W'}$ on a coarse grid, we establish a data-driven model that minimizes the misfit error (i.e., mean squared error) between the predictions from the PeRCNN model and the input measurements. In specific, the loss function is given by

$$\mathcal{L}(\boldsymbol{\theta}) = \text{MSE}\left(\hat{\boldsymbol{\mathcal{U}}}(\tilde{\mathbf{x}}) - \tilde{\mathbf{u}}\right) + \eta \text{MSE}\left(\hat{\boldsymbol{\mathcal{U}}}_0 - \mathcal{I}(\tilde{\mathbf{u}}_0)\right). \tag{5}$$

Note that the first part in RHS of Eq. (5) is adopted for training the network based on the LR measurements $\tilde{\mathbf{u}}$. Herein, $\hat{\boldsymbol{\mathcal{U}}}(\tilde{\mathbf{x}})$ denotes the mapping of HR prediction $\hat{\boldsymbol{\mathcal{U}}} \in \mathbb{R}^{n_t \times H \times W}$ on the grid of measurement data $\tilde{\mathbf{x}}$. Besides, the second part is the regularizer term referring to the discrepancy of interpolated initial state $\mathcal{I}(\tilde{\mathbf{u}}_0)$ and the prediction from ISG. The introduction of the IC regularizer is due to its effectiveness in avoiding the model overfitting. Moreover, η is the weighting coefficient for balancing these two loss components in the model training.

Sparse regression. With the reconstructed high-fidelity (i.e., HR and denoised) solution, we are able to reliably and accurately perform sparse regression for the explicit form of PDEs. As described in Section 3.3, given a library of candidate functions $\boldsymbol{\Theta}(\mathbf{U})$, sparse regression seeks to find a suitable coefficient vector $\boldsymbol{\Xi}$ that balances model complexity and accuracy. This is realized by solving the optimization problem described by Eq. (4) with the STRidge algorithm.

Fine-tuning of coefficients. The obtained coefficients from sparse regression may not fully exploit all the available measurement as the regression is performed on subsampled data. To further improve the result of equation discovery, we present a fine-tuning step to produce the final explicit governing equation. In the fine-tuning step, all the spatiotemporal measurements are used to train a recurrent

block completely based on the identified PDE structure from the sparse regression. The coefficient of each term, which is treated as a trainable variable in the network, can be obtained by minimizing the misfit error between the predictions and measurements. In Appendix Section D, it is demonstrated that the fine-tuning step can effectively improve the accuracy of the discovered PDE.

4 EXPERIMENTS

4.1 DATASETS

To examine the effectiveness of the proposed approach, we test on three different datasets (i.e., PDE systems) which cover the 2D Burgers' equation, 2D Lambda-Omega (λ–Ω) and 2D Gray-Scott (GS) reaction-diffusion (RD) equations. All of them are valuable mathematically and practically, and usually work as the benchmark examples. For instance. 2D Burgers' equation has wide applications in fluid mechanics, acoustics and traffic flow, while the GS RD equation is extensively used to model the process in chemistry and biochemistry. The first PDE system is the 2D Burgers' equation, which has the form of

$$\mathbf{u}_t + \mathbf{u} \cdot \nabla \mathbf{u} = \nu \Delta \mathbf{u} \tag{6}$$

where ∇ is the Nabla operator; Δ is the Laplacian operator; $\mathbf{u} = [u,\ v]^{\mathrm{T}}$ is the fluid velocities and ν is the viscosity coefficient. The second and third RD equation system can both be described by

$$\mathbf{u}_t = \mathbf{D}\Delta\mathbf{u} + \mathbf{R}(\mathbf{u}) \tag{7}$$

where $\mathbf{u} = [u,\ v]^{\mathrm{T}}$ is the concentration vector; $\mathbf{D} = [\mu_u, 0; 0, \mu_v]$ is the diagonal diffusion coefficient matrix; $\mathbf{R}(\mathbf{u})$ denotes the reaction vector. For the λ–Ω RD system, the reaction vector has the form of $\mathbf{R}(\mathbf{u}) = [(1 - u^2 - v^2)u + \beta(u^2 + v^2)v,\ \ -\beta(u^2 + v^2)u + (1 - u^2 - v^2)v]^{\mathrm{T}}$ where β is a reaction parameter. For the GS RD system, the nonlinear reaction vector reads $\mathbf{R}(\mathbf{u}) = [-uv^2 + f(1 - u),\ uv^2 - (f + \kappa)v]^{\mathrm{T}}$ where κ and f denote the kill and feed rate respectively.

4.2 EVALUATION METRIC

We adopt three quantitative metrics to examine the performance of the our approach for discovering PDEs, including:

Relative ℓ_2 error of coefficients. The relative ℓ_2 error, defined as $E = \frac{||\boldsymbol{\Xi}_{\text{id}} - \boldsymbol{\Xi}_{\text{true}}||_2}{||\boldsymbol{\Xi}_{\text{true}}||_2}$, is used to measure the relative distance between the identified coefficient vector $\boldsymbol{\Xi}_{\text{id}}$ and the ground truth $\boldsymbol{\Xi}_{\text{true}}$. However, when the magnitude of coefficients vary significantly, E cannot reflect the result well as the small coefficients get overwhelmed. Hence, we introduce the following non-dimensional measures to gain a more insightful evaluation of the results.

Precision and recall. The equation discovery can also be seen as a binary classification problem (e.g., whether a term exists or not) given a library of candidate functions. Therefore, we present the precision and recall to evaluate the performance of the proposed method. The recall measures the percentage of the successfully identified coefficients among the true coefficients, defined as $R = \frac{||\boldsymbol{\Xi}_{\text{id}} \odot \boldsymbol{\Xi}_{\text{true}}||_0}{||\boldsymbol{\Xi}_{\text{true}}||_0}$ where $\odot$ denotes element-wise product of two vectors[2]. Similarly, the precision, which is defined as $P = \frac{||\boldsymbol{\Xi}_{\text{id}} \odot \boldsymbol{\Xi}_{\text{true}}||_0}{||\boldsymbol{\Xi}_{\text{id}}||_0}$, measures the percentage of correctly identified coefficients among all the identified coefficients.

4.3 EXPERIMENT SETUP

Generation of measurements. The noisy and LR measurements are synthetized through numerical simulations with high-order FD methods. 9-point stencil is used for computing the spatial derivatives while time stepping is performed through Runge-Kutta scheme. For the 2D Burgers' equation system, we select ν to be 0.005 (Geneva & Zabaras, 2020) and generate the solution on a

[2] A "successful" identification of a coefficient occurs when the corresponding entries in both identified and true vector are nonzero.

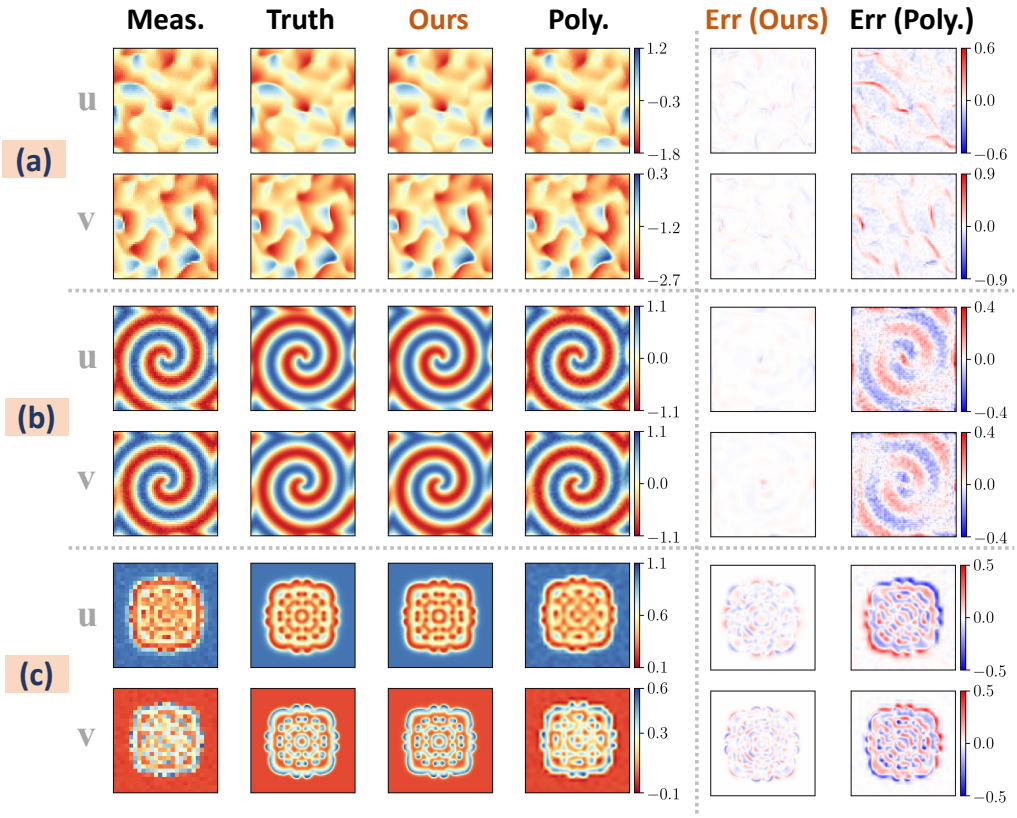

Figure 2: Snapshots of the state variable $[u,\ v]$ at one time instance. (a)-(c) represent the 2D Burgers', λ–Ω and GS RD systems. Four columns starting from the left denote the LR measurement, HR ground truth, reconstructed HR solution from our physics-encoded data-driven model and Chebyshev polynomial fitting (used in PDE-FIND) respectively. The reconstruction error of each model is also provided on the right.

unit square domain discretized by the 101×101 grid. 200 time steps is simulated for a total duration of 0.05 second. The numerical solution is downsampled to measurements as $\tilde{\mathbf{u}} \in \mathbb{R}^{40\times2\times51\times51}$. For the 2D λ–Ω RD system, β, μ_u and μ_v are set to be 1, 0.1 and 0.1 respectively. We discretized the 20×20 square domain with the 101×101 grid. 200 time steps are considered for a physical duration of 2.5 seconds. The measurements are downsampled from the solution to be $\tilde{\mathbf{u}} \in \mathbb{R}^{40\times2\times51\times51}$. For the 2D GS RD system, the solution is generated on the 101×101 grid for a unit square domain using the parameters of $\mu_u = 2 \times 10^{-5}$, $\mu_v = 5 \times 10^{-6}$, $\kappa = 0.06$ and $f = 0.04$. 800 time steps are simulated for the total duration of 400 seconds. The measurements are obtained by downsampling the numerical solution to $\tilde{\mathbf{u}} \in \mathbb{R}^{160\times2\times26\times26}$. Periodic boundary condition is adopted for all three systems. In addition, to mimic the measurement noise in the real world, we add the Gaussian noise of a given level (e.g., 5% and 10%) to the numerical solution before downsampling for the LR data.

Baselines. In the numerical experiments, we compare our proposed method with the widely used PDE-FIND (Rudy et al., 2017) on several multi-dimensional PDE systems. Different from the settings in (Rudy et al., 2017), here we assume only LR measurements are available for computing the derivatives in $\mathbf{\Theta}(\mathbf{U})$. Specifically, the FD method is used to obtain the derivatives for noise-free data. However, in the case that data is heavily corrupted by noise, the derivatives of the fitted Chebyshev polynomial are used.

Table 1: Summary of the comparison between our proposed framework and PDE-FIND.

Cases	Metrics	Relative ℓ_2 error /$\times 10^{-2}$			Precision /%			Recall /%		
	Noise level	0%	5%	10%	0%	5%	10%	0%	5%	10%
Burgers'	Ours	0.50	0.54	0.59	100	100	100	100	100	100
	PDE-FIND	3.32	36.80	45.09	75	100	62.5	100	83.3	83.3
λ–Ω RD	Ours	1.18	2.69	5.44	100	100	91.6	100	100	100
	PDE-FIND	1.70	92.52	99.15	100	83.3	77.8	100	62.5	58.3
GS RD	Ours	1.59	2.85	10.03	100	100	87.5	100	100	87.5
	PDE-FIND	113.05	89.99	108.1	45.5	50.0	42.9	85.7	57.1	60.0

4.4 RESULTS

2D Burgers' equation. We first test the proposed approach on the 2D Burgers' equation. To reconstruct the high-fidelity data, we use the PeRCNN with 3 parallel Conv layers, each of which features 16 channels and filter size of 5. These hyperparameters of network architecture are selected through hold-out validation. The range for selecting the network hyperparameters are given in Appendix Section B. In addition, we assume the measurement exhibits the ubiquitous diffusion phenomenon. That said, the diffusion layer would be encoded into the network architecture. Also in the sparse regression stage, the coefficient of diffusion term would be exempted from being filtered. We train the network with Adam optimizer for 15,000 iterations. The learning rate is initialized to be 0.002 and decreases to 97% of the previous for every 200 iterations.

Once the training is completed, the high-fidelity solution (i.e., 201 snapshots of 101×101) can be inferred from the trained model. Figure 2(a) provides the snapshots of the reconstructed data under 5% noise, as well as the HR data from the Chebyshev polynomial fitting used by PDE-FIND. It can be seen that our method has a much smaller reconstruction error, which would give rise to more accurate numerical differentiation for the derivatives. To prepare for the subsequent sparse regression, we established a group of 42 candidate functions that consists of polynomial terms $\{1, u, v, u^2, uv, v^2\}$, derivatives $\{1, u_x, u_y, v_x, v_y, \Delta u, \Delta v\}$ and their combinations. We randomly subsample 10% of the reconstructed data for the sparse regression. Note that the selection of the crucial hyperparameter γ in sparse regression is conducted through Pareto analysis, which is detailed in Appendix Section E. In addition to the diffusion terms known $a\ priori$, the result of sparse regression (5% noise case) indicates the presence of several other terms in $\mathcal{F}$, i.e., $\mathcal{S}_u = \{uu_x, vu_y\}$ and $\mathcal{S}_v = \{uv_x, vv_y\}$ respectively. As the last step, the fine-tuning is performed using the network built completed based on the discovered PDE structure in the second stage (see Fig. 1(3b)), which gives us the final discovered equation

$$\begin{aligned} u_t &= -5.0113 \times 10^{-3} \Delta u + 1.004 u u_x + 1.004 v u_y, \\ v_t &= -4.9953 \times 10^{-3} \Delta v + 1.009 u v_x + 1.002 v v_y. \end{aligned} \tag{8}$$

The precision, recall and relative ℓ_2 error of the discovered PDE under various noise levels are provided in Table 1. It can be observed that both methods perform well when the measurement is noise-free. However, the result of PDE-FIND deteriorates sharply as the noise level increases while our approach demonstrates much better robustness against the noise. The proposed approach achieves 5.9×10^{-3} relative ℓ_2 error, 100% recall and precision under the 10% noise level.

2D λ–Ω RD equation. The second example is the 2D λ–Ω RD system. The recurrent network employed in the data reconstruction has 3 parallel Conv layers, 16 channels, 5×5 kernels. The highway diffusion Conv layer is constructed to account for the assumption of existing diffusion term. The same routine in previous example for training the reconstruction network is adopted here. Once the training is completed, we infer from the network the high-fidelity (200 snapshots of 101×101 resolution) solution at finer spatiotemporal grid. The reconstruction error of our method and the PDE-FIND is shown in Fig. 2(b). In the library matrix $\mathbf{\Theta}(\mathbf{U})$ with 70 candidate functions for sparse regression, we considered polynomial terms $\{1, u, v, u^2, uv, v^2, u^3, u^2v, uv^2, v^3\}$, derivatives $\{1, u_x, u_y, v_x, v_y, \Delta u, \Delta v\}$ and their combinations. We randomly subsample 10% of the HR points for the sparse regression, whose result (5% noise case) gives the set of terms with nonzero

coefficients, i.e., $\mathcal{S}_u = \{\Delta u, u, u^3, u^2v, uv^2, v^3\}$ and $\mathcal{S}_v = \{\Delta v, u, u^3, u^2v, uv^2, v^3\}$. With the set of existing terms in the governing PDE, the fine-tuning step is performed using all the available measurement. The obtained scalar coefficients from the fine-tuning renders us with the final governing equation, which reads as

$$\begin{aligned} u_t =& 0.096\Delta u + 1.038u - 1.048u^3 + 1.004u^2v - 1.050uv^2 + 0.998v^3, \\ v_t =& 0.100\Delta v + 1.014v - 0.998u^3 - 1.025u^2v - 0.999uv^2 - 1.015v^3. \end{aligned} \tag{9}$$

The evaluation metrics computed from the discovered PDE under various noise level are provided in Table 1. Our approach achieves 5.44×10^{-2} relative error, 100% recall and 91.6% precision in the case of 10% noise.

2D GS RD equation. We consider the 2D GS RD equation system as the last example. In this problem, we assume the measurements are some extremely LR (i.e., 26×26) snapshots (see measurements in Fig. 2). To remedy the lack of resolution in spatial dimension, we further introduce the assumption that reaction term is in the form of polynomial after reviewing the existing literatures. As the first step, we employ the network with 3 parallel Conv layers, 8 channels and filter size of 1 to reconstruct the data. Similar to the previous two examples, the recurrent network features a highway diffusion Conv layer. From the reconstruction model, we infer the HR ($\mathbf{u} \in \mathbb{R}^{101\times101}$) solution at finer time instances. Snapshots of HR solution in Fig. 2(c) show our method is able to restore the high-fidelity data from the LR and noisy measurement very well. With the HR solution, a library of polynomials up to the third degree $\mathbf{\Theta}(u, v) = [1, u, v, u^2, uv, v^2, u^3, u^2v, uv^2, v^3]$ is constructed for sparse discovery. We subsample 10% HR data for the sparse regression, which gives us the remaining terms $\mathcal{S}_u = \{\Delta u, 1, u, uv^2\}$ and $\mathcal{S}_v = \{\Delta v, v, uv^2\}$. With the existing terms in the governing equation, we perform the fine-tuning using the completely physics-based Conv block. The final obtained governing equation in the case of 5% noise is

$$\begin{aligned} u_t =& 2.001 \times 10^{-5}\Delta u - 1.003uv^2 - 0.04008u + 0.04008, \\ v_t =& 5.042 \times 10^{-6}\Delta v + 1.009uv^2 - 0.1007v. \end{aligned} \tag{10}$$

As presented in Table 1, our proposed approach performs well on discovering the PDE as a result of fully utilizing the prior physics knowledge, while PDE-FIND struggles due to the extremely LR measurements.

5 Conclusion

We propose a hybrid framework for discovering nonlinear PDE systems from scarce and noisy measurement data, which couples the novel network architecture PeRCNN for the data-driven modeling of dynamical systems and the sparse regression for distilling the dominant candidate functions and coefficients. First of all, one major innovation of our framework to scientific discovery comes from the nonlinearity achieved by the element-wise product operation and its powerful expressiveness (see Appendix Section A) for the nonlinear function $\mathcal{F}(\cdot)$ in PDEs. Besides, our network also features the capability to encode prior physics knowledge via a highway Conv layer that helps to overcome the challenges brought by the scarcity and noise of the measurements. Secondly, we successfully marry PeRCNN to the sparse regression algorithm to solve the crucial equation discovery issues. The coupled scheme enables us to iteratively optimize the network parameters, and fine-tune the discovered PDE structures and coefficients. Through the numerical validation, we demonstrate the superior reconstruction capability and excellent discovery accuracy of our proposed framework against the baseline approach. Overall, we provide an effective, interpretable and flexible approach to accurately and reliably discover the underlying physical laws from the imperfect and coarse-meshed measurements.

References

Yohai Bar-Sinai, Stephan Hoyer, Jason Hickey, and Michael P Brenner. Learning data-driven discretizations for partial differential equations. *Proceedings of the National Academy of Sciences*, 116(31):15344–15349, 2019.

Peter W Battaglia, Jessica B Hamrick, Victor Bapst, Alvaro Sanchez-Gonzalez, Vinicius Zambaldi, Mateusz Malinowski, Andrea Tacchetti, David Raposo, Adam Santoro, Ryan Faulkner, et al.

Relational inductive biases, deep learning, and graph networks. *arXiv preprint arXiv:1806.01261*, 2018.

Filipe de Avila Belbute-Peres, Thomas Economon, and Zico Kolter. Combining differentiable pde solvers and graph neural networks for fluid flow prediction. In *International Conference on Machine Learning*, pp. 2402–2411. PMLR, 2020.

Josh Bongard and Hod Lipson. Automated reverse engineering of nonlinear dynamical systems. *Proceedings of the National Academy of Sciences*, 104(24):9943–9948, 2007.

Michael M Bronstein, Joan Bruna, Yann LeCun, Arthur Szlam, and Pierre Vandergheynst. Geometric deep learning: going beyond euclidean data. *IEEE Signal Processing Magazine*, 34(4):18–42, 2017.

Steven L Brunton, Joshua L Proctor, and J Nathan Kutz. Discovering governing equations from data by sparse identification of nonlinear dynamical systems. *Proceedings of the national academy of sciences*, 113(15):3932–3937, 2016.

Jared L Callaham, Kazuki Maeda, and Steven L Brunton. Robust flow reconstruction from limited measurements via sparse representation. *Physical Review Fluids*, 4(10):103907, 2019.

Zhao Chen, Yang Liu, and Hao Sun. Physics-informed learning of governing equations from scarce data. *arXiv preprint arXiv:2005.03448*, 2020.

Miles D. Cranmer, Alvaro Sanchez-Gonzalez, Peter W. Battaglia, Rui Xu, Kyle Cranmer, David N. Spergel, and Shirley Ho. Discovering symbolic models from deep learning with inductive biases. In *NeurIPS*, 2020.

Saso Dzeroski and Ljupco Todorovski. Discovering dynamics: from inductive logic programming to machine discovery. *Journal of Intelligent Information Systems*, 4(1):89–108, 1995.

N Benjamin Erichson, Lionel Mathelin, Zhewei Yao, Steven L Brunton, Michael W Mahoney, and J Nathan Kutz. Shallow neural networks for fluid flow reconstruction with limited sensors. *Proceedings of the Royal Society A*, 476(2238):20200097, 2020.

Soheil Esmaeilzadeh, Kamyar Azizzadenesheli, Karthik Kashinath, Mustafa Mustafa, Hamdi A Tchelepi, Philip Marcus, Mr Prabhat, Anima Anandkumar, et al. Meshfreeflownet: a physics-constrained deep continuous space-time super-resolution framework. In *SC20: International Conference for High Performance Computing, Networking, Storage and Analysis*, pp. 1–15. IEEE, 2020.

Mojtaba F Fathi, Ali Bakhshinejad, Ahmadreza Baghaie, David Saloner, Raphael H Sacho, Vitaliy L Rayz, and Roshan M D'Souza. Denoising and spatial resolution enhancement of 4d flow mri using proper orthogonal decomposition and lasso regularization. *Computerized Medical Imaging and Graphics*, 70:165–172, 2018.

Kai Fukami, Koji Fukagata, and Kunihiko Taira. Machine-learning-based spatio-temporal super resolution reconstruction of turbulent flows. *Journal of Fluid Mechanics*, 909, 2021.

Han Gao, Luning Sun, and Jian-Xun Wang. Phygeonet: physics-informed geometry-adaptive convolutional neural networks for solving parameterized steady-state pdes on irregular domain. *Journal of Computational Physics*, 428:110079, 2021a.

Han Gao, Luning Sun, and Jian-Xun Wang. Super-resolution and denoising of fluid flow using physics-informed convolutional neural networks without high-resolution labels. *Physics of Fluids*, 33(7):073603, 2021b.

Han Gao, Matthew J Zahr, and Jian-Xun Wang. Physics-informed graph neural galerkin networks: A unified framework for solving pde-governed forward and inverse problems. *arXiv preprint arXiv:2107.12146*, 2021c.

Nicholas Geneva and Nicholas Zabaras. Modeling the dynamics of pde systems with physics-constrained deep auto-regressive networks. *Journal of Computational Physics*, 403:109056, 2020.

Vincent Le Guen and Nicolas Thome. Disentangling physical dynamics from unknown factors for unsupervised video prediction. In *Proceedings of the IEEE/CVF Conference on Computer Vision and Pattern Recognition*, pp. 11474–11484, 2020.

Jiequn Han, Arnulf Jentzen, and E Weinan. Solving high-dimensional partial differential equations using deep learning. *Proceedings of the National Academy of Sciences*, 115(34):8505–8510, 2018.

George Em Karniadakis, Ioannis G Kevrekidis, Lu Lu, Paris Perdikaris, Sifan Wang, and Liu Yang. Physics-informed machine learning. *Nature Reviews Physics*, 3(6):422–440, 2021.

Samuel Kim, Peter Y Lu, Srijon Mukherjee, Michael Gilbert, Li Jing, Vladimir Čeperić, and Marin Soljačić. Integration of neural network-based symbolic regression in deep learning for scientific discovery. *IEEE Transactions on Neural Networks and Learning Systems*, 2020.

Thomas N Kipf and Max Welling. Semi-supervised classification with graph convolutional networks. *arXiv preprint arXiv:1609.02907*, 2016.

Dmitrii Kochkov, Jamie A Smith, Ayya Alieva, Qing Wang, Michael P Brenner, and Stephan Hoyer. Machine learning–accelerated computational fluid dynamics. *Proceedings of the National Academy of Sciences*, 118(21), 2021.

Isaac E Lagaris, Aristidis Likas, and Dimitrios I Fotiadis. Artificial neural networks for solving ordinary and partial differential equations. *IEEE transactions on neural networks*, 9(5):987–1000, 1998.

Hyuk Lee and In Seok Kang. Neural algorithm for solving differential equations. *Journal of Computational Physics*, 91(1):110–131, 1990.

Jun Li, Gan Sun, Guoshuai Zhao, and Li-Wei H. Lehman. Robust low-rank discovery of data-driven partial differential equations. In *AAAI*, pp. 767–774. AAAI Press, 2020a.

Yunzhu Li, Jiajun Wu, Russ Tedrake, Joshua B Tenenbaum, and Antonio Torralba. Learning particle dynamics for manipulating rigid bodies, deformable objects, and fluids. *arXiv preprint arXiv:1810.01566*, 2018.

Zongyi Li, Nikola Kovachki, Kamyar Azizzadenesheli, Burigede Liu, Kaushik Bhattacharya, Andrew Stuart, and Anima Anandkumar. Fourier neural operator for parametric partial differential equations. *arXiv preprint arXiv:2010.08895*, 2020b.

Min Lin, Qiang Chen, and Shuicheng Yan. Network in network. *arXiv preprint arXiv:1312.4400*, 2013.

Bo Liu, Jiupeng Tang, Haibo Huang, and Xi-Yun Lu. Deep learning methods for super-resolution reconstruction of turbulent flows. *Physics of Fluids*, 32(2):025105, 2020.

Zichao Long, Yiping Lu, Xianzhong Ma, and Bin Dong. Pde-net: Learning pdes from data. In *International Conference on Machine Learning*, pp. 3208–3216. PMLR, 2018.

Zichao Long, Yiping Lu, and Bin Dong. Pde-net 2.0: Learning pdes from data with a numeric-symbolic hybrid deep network. *Journal of Computational Physics*, 399:108925, 2019.

Lu Lu, Pengzhan Jin, Guofei Pang, Zhongqiang Zhang, and George Em Karniadakis. Learning nonlinear operators via deeponet based on the universal approximation theorem of operators. *Nature Machine Intelligence*, 3(3):218–229, 2021.

Ravi G Patel, Nathaniel A Trask, Mitchell A Wood, and Eric C Cyr. A physics-informed operator regression framework for extracting data-driven continuum models. *Computer Methods in Applied Mechanics and Engineering*, 373:113500, 2021.

Maziar Raissi. Deep hidden physics models: Deep learning of nonlinear partial differential equations. *The Journal of Machine Learning Research*, 19(1):932–955, 2018.

Maziar Raissi, Paris Perdikaris, and George E Karniadakis. Physics-informed neural networks: A deep learning framework for solving forward and inverse problems involving nonlinear partial differential equations. *Journal of Computational Physics*, 378:686–707, 2019.

Chengping Rao, Hao Sun, and Yang Liu. Embedding physics to learn spatiotemporal dynamics from sparse data. *arXiv preprint arXiv:2106.04781*, 2021a.

Chengping Rao, Hao Sun, and Yang Liu. Physics-informed deep learning for computational elastodynamics without labeled data. *Journal of Engineering Mechanics*, 147(8):04021043, 2021b.

Pu Ren, Chengping Rao, Yang Liu, Jianxun Wang, and Hao Sun. Phycrnet: Physics-informed convolutional-recurrent network for solving spatiotemporal pdes. *arXiv preprint arXiv:2106.14103*, 2021.

Samuel H Rudy, Steven L Brunton, Joshua L Proctor, and J Nathan Kutz. Data-driven discovery of partial differential equations. *Science Advances*, 3(4):e1602614, 2017.

Subham Sahoo, Christoph Lampert, and Georg Martius. Learning equations for extrapolation and control. In *International Conference on Machine Learning*, pp. 4442–4450. PMLR, 2018.

Alvaro Sanchez-Gonzalez, Jonathan Godwin, Tobias Pfaff, Rex Ying, Jure Leskovec, and Peter Battaglia. Learning to simulate complex physics with graph networks. In *International Conference on Machine Learning*, pp. 8459–8468. PMLR, 2020a.

Alvaro Sanchez-Gonzalez, Jonathan Godwin, Tobias Pfaff, Rex Ying, Jure Leskovec, and Peter Battaglia. Learning to simulate complex physics with graph networks. In *International Conference on Machine Learning*, pp. 8459–8468. PMLR, 2020b.

Michael Schmidt and Hod Lipson. Distilling free-form natural laws from experimental data. *science*, 324(5923):81–85, 2009.

Karen Stengel, Andrew Glaws, Dylan Hettinger, and Ryan N King. Adversarial super-resolution of climatological wind and solar data. *Proceedings of the National Academy of Sciences*, 117(29): 16805–16815, 2020.

Fangzheng Sun, Yang Liu, and Hao Sun. Physics-informed spline learning for nonlinear dynamics discovery. *arXiv preprint arXiv:2105.02368*, 2021.

Benjamin Ummenhofer, Lukas Prantl, Nils Thuerey, and Vladlen Koltun. Lagrangian fluid simulation with continuous convolutions. In *International Conference on Learning Representations*, 2019.

Rui Wang, Karthik Kashinath, Mustafa Mustafa, Adrian Albert, and Rose Yu. Towards physics-informed deep learning for turbulent flow prediction. In *Proceedings of the 26th ACM SIGKDD International Conference on Knowledge Discovery & Data Mining*, pp. 1457–1466, 2020.

Bing Yu et al. The deep ritz method: a deep learning-based numerical algorithm for solving variational problems. *arXiv preprint arXiv:1710.00211*, 2017.

Yinhao Zhu and Nicholas Zabaras. Bayesian deep convolutional encoder–decoder networks for surrogate modeling and uncertainty quantification. *Journal of Computational Physics*, 366:415–447, 2018.

Yinhao Zhu, Nicholas Zabaras, Phaedon-Stelios Koutsourelakis, and Paris Perdikaris. Physics-constrained deep learning for high-dimensional surrogate modeling and uncertainty quantification without labeled data. *Journal of Computational Physics*, 394:56–81, 2019.

APPENDIX

A Π-BLOCK AS A UNIVERSAL POLYNOMIAL APPROXIMATOR

In the proposed PeRCNN, Π-block acts as an universal polynomial approximator to unknown nonlinear functions while the physics-based highway Conv layer accounts for the prior knowledge on the governing equation. Notably, the Π-block achieves its nonlinearity through the element-wise product operation (see Eq. (2)) instead of what is widely adopted by the traditional Conv network, in which nonlinear layers are sequentially interwined with linear layers. This multiplicative representation promotes the network expressiveness for nonlinear terms, compared with the additive form representation $\mathcal{F}(\mathbf{u}) = \sum_{0\leq i+j\leq N} f_{ij} \cdot (\mathcal{K}_{ij} \circledast \mathbf{u})$ commonly seen in related work (Long et al., 2018; Guen & Thome, 2020). To support this claim, we need to recognize that Π-block roots on the numerical differentiation (i.e., forward Euler time stepping), which can guarantee the convergence of the solution under two conditions: (i) the RHS $\mathcal{F}$ of Eq. (1) can be computed accurately; and (ii) the time spacing δt is sufficiently small. As the second condition can be satisfied by selecting an appropriate δt, we would show that, by construction, our Π-block can approximate any nonlinear polynomial involving spatial derivatives, such as $uu_x + vu_y$ and $u\Delta u$. This can be easily argued by proving that each monomial (e.g., uu_x, vu_y, etc.) can be approximated by multiplying the output of given number of Conv layers. To this end, we provided the following lemma and its proof reproduced from (Long et al., 2019).

Lemma 1: By construction, a convolutional filter $\mathcal{K}$ with a given size can approximate any differential operator with prescribed order of accuracy.

Proof 1: Without loss of generality, let us consider a bivariate differential operator $\mathcal{L}(\cdot)$ w.r.t variables x and y, we have

$$
\begin{aligned}
\mathcal{L}(u) &= \sum_{k_1,k_2=-\frac{N-1}{2}}^{\frac{N-1}{2}} \mathcal{K}[k_1,k_2] \sum_{i,j=0}^{N-1} \frac{\partial^{i+j}u}{\partial^i x \partial^j y}\bigg|_{(x,y)} \frac{k_1^i k_2^j}{i!j!} \delta x^i \delta y^j + \mathcal{O}(|\delta x|^{N-1} + |\delta y|^{N-1}) \\
&= \sum_{k_1,k_2=-\frac{N-1}{2}}^{\frac{N-1}{2}} \mathcal{K}[k_1,k_2] u(x+k_1\delta x, y+k_2\delta y) + \mathcal{O}(|\delta x|^{N-1} + |\delta y|^{N-1}) \\
&= \mathcal{K} \circledast u + \mathcal{O}(|\delta x|^{N-1} + |\delta y|^{N-1})
\end{aligned}
\tag{11}
$$

where N is the size of the filter. The weight matrix $\mathcal{K}[\cdot,\cdot]$ is indexed by k_1 and k_2. Letting the filter's entry $\mathcal{K}[k_1,k_2]$ be the corresponding Taylor series coefficient, we can see the approximation error is bounded by $\mathcal{O}(|\delta x|^{N-1} + |\delta y|^{N-1})$.

B HYPERPARAMETER SELECTION OF PERCNN IN DATA RECONSTRUCTION

The selection of the hyperparameters of PeRCNN for data reconstruction is performed through the hold-out validation. Among the entire measurement, 10% data is split as the validation dataset. The range of hyperparameters we considered are summarized in Table B.1. The value in the parenthesis denotes the final parameter adopted in the data reconstruction.

C ENCODE PHYSICS KNOWLEDGE TO ENHANCE THE MODEL

As introduced in Section 3.2, one salient characteristic of the proposed network is the capability to encode prior physics knowledge. To examine how the encoded physics enhances the accuracy of the data-driven model, here we use the 2D Burgers' equation system as a testbed. In the experiment, we consider two different cases: (1) no prior knowledge is available, and (2) the diffusion term ($\Delta\mathbf{u}$) is known to exist in $\mathcal{F}$. The setting in the second case leads to an additional physics-based Conv layer

Table B.1: Range of hyperparameters for the data reconstruction network.

Dataset	Kernel size	# layers	# channels	Learning rate	Regularizer weight η
2D Burgers'	1∼5 (5)	2∼4 (3)	4∼16 (16)	0.001∼0.01 (0.002)	0.001∼1 (1)
2D λ–Ω	1∼5 (5)	2∼4 (3)	4∼16 (16)	0.001∼0.01 (0.002)	0.001∼1 (0.01)
2D GS	1∼5 (1)	2∼4 (3)	4∼16 (8)	0.001∼0.01 (0.001)	0.001∼1 (0.005)

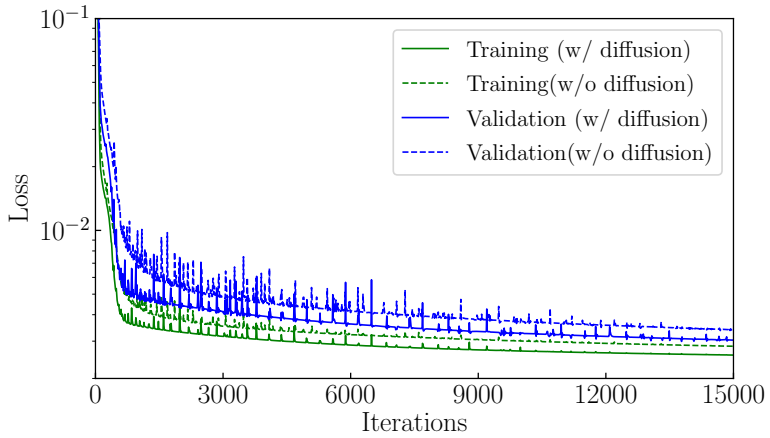

Figure C.1: Learning curve of the data-driven model with (w/) and without (w/o) encoded diffusion layer for 15,000 iterations.

in PeRCNN to account for the diffusion term. Apart from this, other hyperparameters are kept same in the experiment.

Figure C.1 shows the learning curves of these two data-driven models. It can be observed that the network encoded with the diffusion term exhibits faster convergence and better accuracy compared with the competitor. As a result of encoding prior physics knowledge, the PeRCNN does not need to learn a diffusion operator through the back propagation of error. That said, incorporating available physics can facilitate the learning efficiency and accuracy of the data-driven model.

D Importance of the coefficient fine tuning

Our proposed approach for discovering PDEs consists of three stages including the data reconstruction, the sparse regression and the fine-tuning of coefficients. In fact, the sparse regression has already been able to determine the explicit form of the discovered PDE. Then a natural question would be why the last fine-tuning step is necessary. As its name indicates, the fine-tuning step is able to further improve the accuracy of the discovered PDE, for mainly two reasons: (i) The sparse regression step gives an explicit PDE based on the primitive assumption of a sparse $\boldsymbol{\Xi}$. However, the discovered PDE can be further considered as the latest assumption, based on which a completely physics-based recurrent network can be established. In the fine-tuning step, the functional form of the PDE is unchanged while its scalar coefficients are optimized. That said, the fine-tuning step is an optimization process on a much smaller parameter space. (ii) The sparse regression is performed on subsampled high-dimensional spatiotemporal data while the fine-tuning step could utilize all the available measurement through the recurrent network.

The above argument provides some intuitions of the coefficient fine-tuning step. To further justify it, we compute the relative ℓ_2 error of the coefficient vector before/after the fine-tuning step, which is given in Table D.1. It can be seen that fine-tuning step improves the accuracy of the discovered PDE consistently for different noise level. Interestingly, we observe that for the 2D GS and λ–Ω RD case under 10% noise, the improvement brought by the fine tuning step is not as evident as that of the other cases. That is because, in these two cases, the sparse regression does not give the correct form

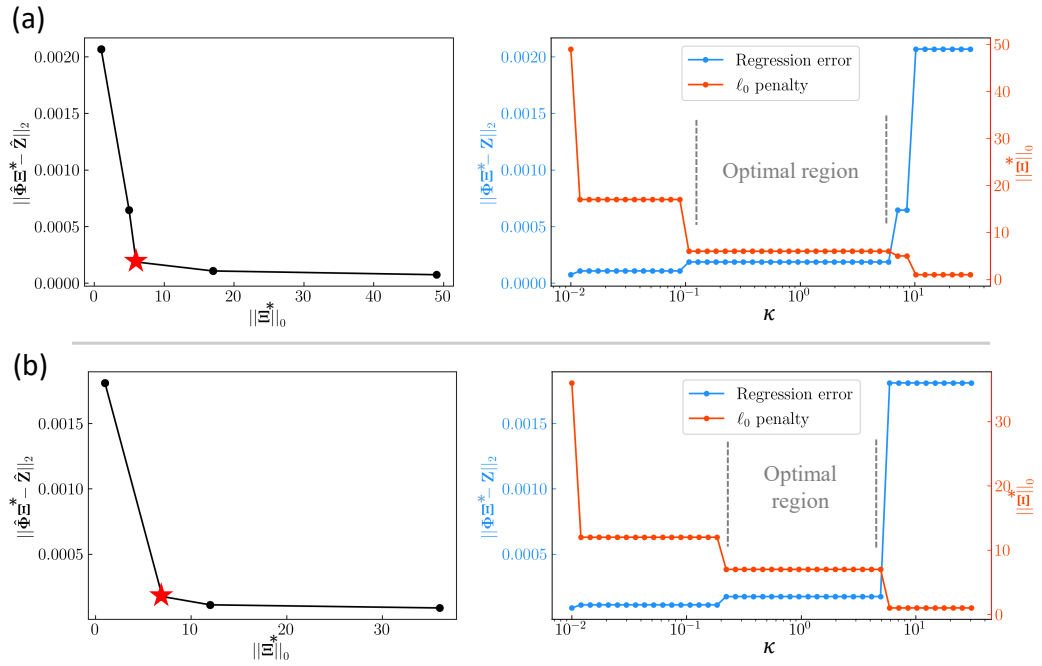

Figure E.1: Pareto analysis for selecting the weighting coefficient κ (or γ) in 2D λ–Ω GS system (10% noise level). (a) and (b) correspond to the $\mathcal{F}_u$ and $\mathcal{F}_v$ respectively. The Pareto front that represents the optimal κ is marked with the red star.

of the PDE. In other words, the fine-tuning is performed based on an assumption that deviates from the fact. The dependency on the sparse regression result also implies one limitation of our approach.

Table D.1: Relative ℓ_2 error (unit: 10^{-2}) of the coefficient vector before and after the fine tuning.

Case	Stage	Noise level		
		0%	5%	10%
Burgers'	Before	0.93	1.57	2.18
	After	0.50	0.54	0.59
λ–Ω RD	Before	1.52	3.33	6.65
	After	1.18	2.69	5.44
GS RD	Before	6.40	9.84	12.33
	After	1.59	2.85	10.03

E PARETO ANALYSIS FOR HYPERPARAMETER SELECTION

As introduced in Section 3.3, sparse regression is formulated as an optimization problem described by Eq. (4). The aggregated optimization objective consists of two components, $||\mathbf{U}_t - \mathbf{\Theta}(\mathbf{U})\mathbf{\Xi}||_2$ and $||\mathbf{\Xi}||_0$, to ensure the accuracy of the regression while keeping the model parsimonious. This trade-off can be balanced by selecting an appropriate weighting coefficient γ in the aggregated objective function. Pareto analysis is so far considered as the most effective way for selecting this hyperparameter γ. To ensure the scale of two components aligned, we introduce an equivalent hyperparameter κ as the nondimensional weighting coefficient. The κ and γ are interconvertible with the definition $\gamma \equiv \kappa||\mathbf{U}_t - \mathbf{\Theta}(\mathbf{U})\tilde{\mathbf{\Xi}}||_2$ where $\tilde{\mathbf{\Xi}}$ is the Least Squares solution to the linear system.

In the Pareto analysis, we would sample some points of κ from $[10^{-2},\ 20]$. For each of the point, we would pass it as the argument for the sparse regression routine, which would return the optimal coefficient vector $\boldsymbol{\Xi}^*$. The corresponding regression error and ℓ_0 penalty can be computed for Pareto analysis. Figure E.1 provides the results of Pareto analysis for 2D λ–Ω equation system (10% noise case). From the subfigure on the left, we can identify the Pareto front that corresponds to the optimal region of κ. Pareto analyses as such are performed on each case to find the suitable weighting coefficient κ (or equivalently γ). The value of κ employed in each case is summarized in Table E.1.

However, readers should note that the Pareto front may not always be so obvious to identify. In many scenarios, trade-off between the model sparsity and accuracy must be done with manual selection, which still appears to be more art than science.

Table E.1: The coefficient κ employed in sparse regression.

Method	Burgers'			λ–Ω RD			GS RD		
	0%	5%	10%	0%	5%	10%	0%	5%	10%
Ours	1	1	1	1	1	1	0.1	0.1	1
PDE-FIND	1	1	1	1	1	1	0.1	0.05	0.1